

Full length article

Fast analogue 2π phase modulation using a liquid crystal Pi-CellLinpei Xue, Yihan Jin, Steve J. Elston, Stephen M. Morris^{*}

Department of Engineering Science, University of Oxford, Parks Road, Oxford, OX1 3JP, United Kingdom

ARTICLE INFO

Keywords:

Nematic liquid crystal
Phase modulator
Spatial light modulator
Optical phase measurement
Liquid crystal pi-cell

ABSTRACT

In this paper, we investigate the optical phase modulation potential of a nematic liquid crystal (LC) pi-cell operating in the so-called symmetric H (Hs) state. Experimental results of the optical phase modulation obtained using a phase-shifting Michelson interferometer are presented which are then compared with results from simulations carried out using Ericksen-Leslie continuum theory. The stability of the Hs state, which is limited, is investigated by adjusting the amplitude of the applied voltage and the duration of the voltage burst. To achieve full 2π phase modulation with 1 ms timescale in a reflective geometry (akin to that of a spatial light modulator), we employ a short burst voltage to drive the LC pi-cell into the Hs state, which shows excellent phase modulation capability, and the experimental results are found to be in good agreement with the results from simulations.

1. Introduction

The need for high performance displays [1] and image projection [2] has been a key driver in the development of liquid crystal (LC) spatial light modulator (SLM) technology for applications requiring high frame rate and analogue 2π phase modulation at low driving voltages [3]. For nematic LC-based SLM technologies, previous developments in this field have typically resulted in response times of the order of milliseconds, limited for the most part by the viscoelastic response of the nematic LC [4]. To enable SLM technology to be used in a wider range of applications, such as LiDAR and optical beamsteering [5], super-resolution optical microscopy [6,7], optically probing of biological systems [8] and holography [9,10], improving the switching speed while maintaining access to the full 2π range is of great necessity.

Currently, LC-based SLMs typically employ either a ferroelectric liquid crystal (FLC) or a nematic LC (NLC) to modulate the optical phase. However, both FLC and NLC technologies have their pros and cons. For example, FLC-based SLM technology exhibits a fast response time (generally of the order of sub-milliseconds), but the phase modulation is usually only binary [11,12], which requires sophisticated optical configurations to generate a continuous phase modulation [13,14]. Nematic SLM technology, on the other hand, does exhibit multi-level analogue phase modulation, but at the expense of a slower response time. Other LC modes do exist that can exhibit both fast response and analogue phase modulation, but such modes have not yet been successfully commercialized. For example, both the flexoelectro-optic effect in chiral nematic and the electro-optic switching in nematic pi-cells have the

potential for both fast response and full 2π analogue phase modulation.

In the case of the flexoelectro-optic effect in chiral nematic LCs, fast sub-millisecond response times can be observed when the pitch (p) of the helix is short ($p \approx 300\text{--}400$ nm) [15]. In the uniform lying helix (ULH) geometry, flexoelectric coupling to an applied electric field results in a tilt of the optic axis of the chiral nematic LC in the plane of the device. This rotation of the optic axis can then be manifested as a phase modulation when the LC layer is sandwiched between quarter-wave plates, as demonstrated in [16]. To observe flexoelectro-optic switching, a ULH alignment is required when conventional transverse electric fields are employed (the electric field is aligned along the normal of the device substrates). However, the formation of the ULH alignment is nontrivial [17] and polymer stabilization is often employed to stabilize the alignment, albeit with varying degrees of success [18]. Furthermore, while analogue 2π phase modulation with 1 ms response time has been observed using this electro-optic mode, the device had to be operated at relatively high temperatures in excess of 100 °C [19].

Fast-switching electro-optic effects can be observed in nematic LCs when used in the so-called pi-cell configuration, which consists of parallel rubbed planar alignment layers. In this arrangement, the nematic LC can respond on the order of a few milliseconds or less by virtue of the symmetric LC director profile coupled with the absence of backflow during director reorientation [20,21]. In a pi-cell device, the optically compensated bend (OCB) mode is realized by applying a voltage above a certain threshold [22,23]. However, since there is a topological difference between the relaxed state and the electric field-driven bend state needed for OCB operation, the amplitude of the applied voltage needs to

^{*} Corresponding author.

E-mail address: stephen.morris@eng.ox.ac.uk (S.M. Morris).

<https://doi.org/10.1016/j.optlastec.2023.109773>

Received 5 February 2023; Received in revised form 21 June 2023; Accepted 24 June 2023

Available online 12 July 2023

0030-3992/© 2023 The Author(s). Published by Elsevier Ltd. This is an open access article under the CC BY-NC-ND license (<http://creativecommons.org/licenses/by-nc-nd/4.0/>).

be high enough to initiate the slow nucleation transition (which can take a few seconds) as well as maintain the device in the bend state instead of transforming to a twisted state (T state). In order to maintain the required state, and achieve suitable response times, researchers have proposed the use of polymer stabilization [24,25] or alternatively an

increase in the pretilt angle at the substrates of the device [26,27]. However, polymer stabilization usually also results in an unwanted increase in the switching voltage, and both approaches reduce the overall range of optical phase modulation.

Pi-cell devices exhibit an array of different director configurations

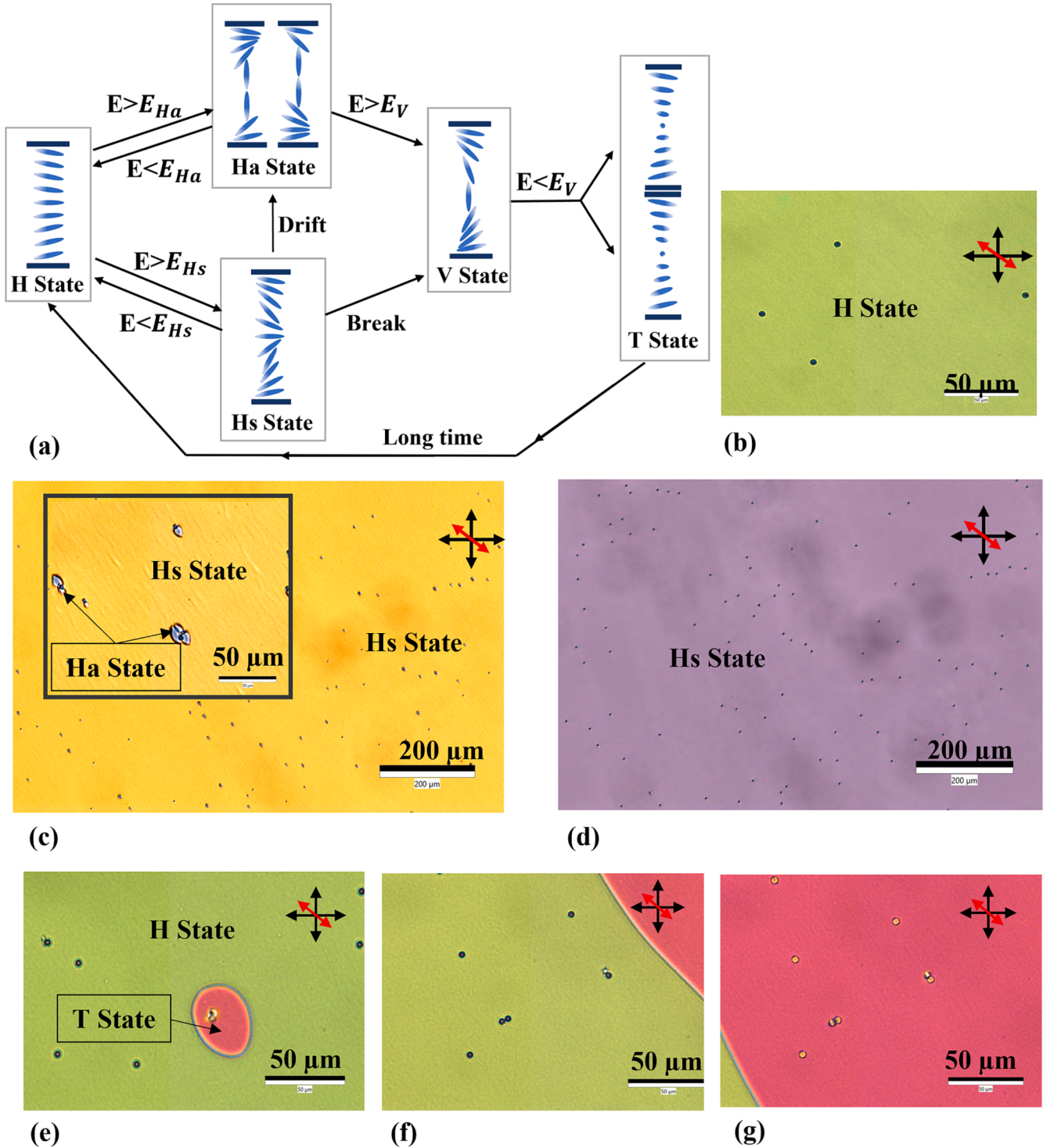


Fig. 1. The switching states of a nematic pi cell. (a) An illustration showing the transitions of a nematic pi-cell under different electric field conditions. Representative polarizing optical microscope (POM) images of (b) the splay state of the device under no applied voltage (the black dots in the image are the spacer beads distributed throughout the cell to obtain a uniform cell gap). (c) mixture of Hs state and Ha states when the device was driven by a burst driving voltage of 4 Vrms for 90 ms. (d) the Hs state formed by a burst driving voltage of 7 Vrms for 20 ms. (e) formation of the V state under a burst voltage of 10 Vrms, and during the relaxation period, V state relaxes to T state while Hs state relaxes to the H state, (f)-(g) demonstrate the growth of the V state under a repeating burst voltage of 10 Vrms for 50 ms. The crossed double-headed black arrows represent the orientations of the transmission axes of the polarizer and the analyzer, and the double-headed red arrow represents the rubbing direction of the alignment layers.

when subjected to an electric field and as a result can be operated in different ‘modes’. One such mode that has received little attention for potential optical phase modulation applications is the symmetric H (Hs) state, which could potentially exhibit continuous (analogue) phase modulation together with sub-millisecond response times at moderate driving voltages [20,28]. This mode therefore warrants further investigation for potential use as an optical phase modulator, and it is this mode that is the focus of the present paper. While many of the characteristics are favourable for phase modulation, the effective lifetime of the Hs state is typically of the order of a hundred milliseconds, which is rather short, and potentially restricts its practical application.

In this paper, we investigate the rapid response mechanism of the Hs state and the potential of this mode in optical phase modulation by applying a burst driving voltage. The experimental result shows that a pi-cell device with a cell gap (LC layer thickness) of 3.7 μm can achieve 2π phase modulation in 1 ms using a10 Vrms burst driving voltage at room temperature – these experimental results are also found to be in good agreement with the results obtained from simulations. In Section 2, the pi-cell states are outlined, and the method used to obtain the Hs state is introduced and the factors affecting the lifetime of the Hs state are also investigated. Then, we employ a model including LC flow to derive a theoretical response time based on the dynamic properties of the Hs state, which indicates the potential for full 2π range phase modulation switching in 1 ms. In Section 3, we discuss an experiment based on a phase-shifting Michelson interferometer to measure the optical phase in the time domain. The principles of this method, and the phase extraction techniques employed in this work, are then presented. With this approach, time-resolved phase modulation of the LC device can be precisely measured, demonstrating the potential for phase modulation applications. Finally, Section 4 presents the measured phase modulation for the Hs state, showing excellent consistency with simulated results.

2. The Hs-state Pi-Cell phase modulator

Fig. 1(a) illustrates the typical transformations between the different states of a pi-cell with a low pretilt angle ($\approx 4 \sim 5^\circ$). With no applied voltage, the LC director forms a stable splay (H) state, which has the minimum energy level. When the applied voltage is above a critical voltage V_{th} (Freed) (V_{th} (Freed) $\approx 1 V_{rms}$), then the internal field is above that required to switch to an asymmetric state ($E > E_{Ha}$) and a Fréedericksz transition occurs, and the director profile transforms into one of the asymmetric H (Ha) states. Alternatively, if a sudden voltage above a higher threshold voltage (V_{th} (Hs)) is applied to the H state, then the internal field is above that required to switch to a symmetric state ($E > E_{Hs}$), and the transient Hs state is obtained – this state will tend to drift into the Ha state(s), or transform to the bend state, also termed the vertical (V) state directly for a higher applied voltage.

As the operating voltage is increased above the threshold for the V state, V_{th} (V), then the internal field is increased above that required to switch to a V state ($E > E_V$), and both Hs and Ha states will transform to the V state because the V state is energetically favourable at high voltages. It is worth noting that the transition speed from the Hs state to the V state is much faster than that from the Ha state to the V state due to the larger energy difference between the two states [29], which contributes to the short lifetime of the Hs state. Moreover, when the voltage is removed and the device is in either the Ha or Hs state, the director alignment will return to the H state directly; on the contrary, when removing the voltage in the V state, then a twisted state (T state) forms and the device gradually returns to the H state via domain growth over the course of a few seconds.

Additionally, it can be seen from the schematic in Fig. 1(a) that in the Hs state the LC director in the middle of the device is aligned parallel to the substrates, and the whole device could be regarded as two half thickness Fréedericksz devices stacked together. Consequently, the threshold voltage for the Hs state is double that of the Fréedericksz (antiparallel rubbed alignment layers) device (V_{th} (Hs) $\approx 2 \times V_{th}$

(Freed)). Furthermore, because the response time of Fréedericksz devices is proportional to the square of the LC layer thickness ($\tau \propto d^2$), the response time of the Hs state is more than 4 times faster than the Ha state when considering the additional effects of flow-reorientation coupling [28]. With such potential for fast switching, it is important to investigate the potential of the Hs state in optical phase modulation, but also essential to investigate the stability and the lifetime of the Hs state.

To prolong the lifetime of the Hs state, researchers have proposed that with higher operating voltage, the lifetime of the Hs state will increase [21,30] since higher voltage assists the bulk decoupling from the effects of any asymmetric surface pretilts, which can be the main cause for the director profile collapsing into one of the Ha states. This means higher voltages weaken the impact from any asymmetric surface condition and enables the device to remain in the Hs state longer, and the lifetime of the Hs state will in principle be indefinite if the pretilts of the device are ideally symmetrical. However, Ru Yang et al. have pointed out that under higher applied voltages the V state would tend to rapidly nucleate and cause the device to transition to the OCB mode [31]; therefore, the authors suggested a burst driving method composed of an operating time period and a relaxation time period in order to obtain the Hs state. The operating time needs to be long enough to switch the device to the Hs state but short enough to avoid the device breaking down to the Ha state or transitioning to the V state, and the relaxation time allows a complete recovery to the ground H state.

A. Burst driving the Various States of a Pi-Cell

As noted above, the transient Hs state is obtained by applying a sudden voltage above its threshold, (V_{th} (Hs)). Here, in order to avoid it collapsing to either the Ha state or nucleating to the V state, a burst driving method was adopted to switch the Hs state. The operating period (when the burst voltage is applied) encourages the formation of the Hs state and aims to avoid transformation to other states whereas the relaxation period (when no voltage is applied) ensures a recovery to the ground H state. Then, by repeating the burst voltage periodically, a stable Hs state is obtained regularly. It is found that the amplitude and duration of the operating burst voltage affects the lifetime of the Hs state, thus it is important to study the stability of the symmetric H (Hs) state in order to determine the operating lifetime.

The pi-cell device used in the experiment reported here consisted of glass substrates that were coated with indium tin oxide (ITO) electrodes and parallel rubbed polyimide alignment layers. The surface pretilts were typically within 4° to 5° and the cell gap was 3.7 μm . The nematic LC mixture, E7 (Synthon Ltd.), which has been extensively characterized in terms of its physical properties, was capillary filled into the pi-cell device. To distinguish the transformation between different states, the device was positioned between crossed polarizers on a polarizing optical microscope (POM) (Olympus BX51), with the rubbing direction (optic axis) aligned at 45° to the polarizer and analyzer pair. The applied voltage was a square wave of 1 kHz with a variable burst duration repeated every 1 s. By adjusting the amplitude and burst operating time, the Ha, Hs and V states appear separately, while in some case these states appear together due to the nonuniform conditions of the device substrate surfaces. It should be noted that since there are many spacer beads in the device (used to maintain a uniform cell gap), in practice most of the Ha states and V states form and grow from around these spacer beads.

Fig. 1 demonstrates the switching processes in a pi-cell along with exemplar POM images of the various states. When a continuous driving waveform was applied to the device, the Ha and V states could be observed under lower and higher voltages respectively, but the Hs could not be observed due to its transient lifetime. Both the Ha and V states generally exhibit a uniform colour in the image, although with imperfect surface alignments, several domain walls were seen when the Ha state was formed – caused by the twist and bend of the LC director between neighbouring differing Ha states [32], where the direction of the domain

wall was predominantly aligned with the rubbing direction. However, when the burst driving voltage was applied to the device in order to generate an Hs state, the situation becomes more complicated, and a mixture of states appeared. For example, when the operating condition was a driving burst voltage of 90 ms duration with an amplitude of 4 Vrms, even though the Ha state can still collapse during the relaxation period between the voltage bursts, the formation of the Ha state was still evident, which is not appropriate for a phase modulator design based on the Hs state. The formation of these states is shown in the microscope images in Fig. 1(c) where the Hs state is a yellow colour that dominates the image. However, the Ha state has also formed, which is evidenced by the small blue regions that exist around some of the spacer beads.

In contrast, under a relatively low amplitude voltage and/or short operating time, the Hs state can be obtained on its own, as shown in Fig. 1(d) for a 20 ms duration voltage burst with a voltage amplitude of 7 Vrms. In such a case, a few very small Ha states may still appear due to the asymmetric surface conditions, but because the total area of any Ha state domain forming over the whole device is very small and any Ha states disappear completely at the end of the relaxation period between bursts (due to a decay time of a few milliseconds), any appearance of the Ha states can be ignored. When we further increased the driving amplitude to 10 Vrms, the device exhibited just the Hs state at the beginning of the burst, but as the burst length increased, part of the Hs state transitioned to the V state, which subsequently grew as small regions around the spacer beads. This behaviour can be seen in Fig. 1(e). It should be noted that if the size of the V state regions during this stage is small, and these regions can fully collapse and recover to the ground H state during the relaxation period between bursts, then this has no effect on the Hs formation and modulator design. However, as the burst length increased (i.e., was longer than 35 ms for an applied voltage of 10 Vrms) then the V states grew significantly. In this case they then did not collapse between bursts and consequently the V states continued to grow from burst-to-burst and the whole area of the Hs state eventually transitioned to the V state, as can be seen in Fig. 1(f) and Fig. 1(g).

B. Voltage Conditions for a Stable Hs State

A characterization of the states of the pi-cell device for various applied voltages and duration of the voltage bursts is presented in Fig. 2. These states were determined from observations of the POM images (as illustrated in Fig. 1) together with the measured time-dependent transmission of the device between crossed polarizers. In Fig. 2(a), the applied voltage burst and the corresponding transmission curve measured by placing the device between crossed polarizers with the rubbing direction aligned at 45° to the transmission axis of the polarizers are shown. The operation and relaxation time periods were 30 ms and 970 ms, respectively. Together with the images observed through the

POM, it can be determined that the flat period in the transmission curve during the burst driving period is the Hs state, the constant transmission region during the relaxation period is the ground H state (which is weakly splayed). The undulating transmission(s) between these states then represents the dynamic switching of the device.

By repeating these investigations for a range of voltage bursts and durations, the stable operating regime of the Hs state can be determined, as indicated by the green sections of the vertical bars in Fig. 2(b). The blue areas at the bottom of the bars in Fig. 2(b) represent the time taken for the formation of the Hs state (i.e., the time required to reach equilibrium), acquired from the transmission curve(s). These results show that the time needed for the formation of the Hs state is about 0.2 ~ 5.0 ms for the pi-cell device used in this study, depending on the burst driving voltage applied. It can also be seen that as the voltage increases, the time required to form the Hs state becomes shorter. The green bars indicate the useful lifetime of the Hs state, which tends to decrease as the burst voltage increases. During this time, the formation of a few Ha states might occur around spacer beads, but these are generally small enough to be ignored.

The yellow bars indicate where a mixture of Hs and V state tends to occur, since the duration of the driving burst is sufficient to enable the formation and some growth of the V state, although the V states which have appeared in the yellow bar area are sufficiently small to collapse completely during the relaxation period between bursts, and therefore will not affect the formation of the Hs state in the next voltage burst. This observation indicates that the voltage burst regime in the region of the bars coloured yellow could also potentially be adopted for phase modulator design based on the formation of the Hs states, although, clearly as the drive voltage increases, the burst duration should decrease so as to maintain an Hs state that is sufficiently stable to be of use. Moreover, the red areas indicate the condition when the V state continues to grow as the voltage bursts repeat (instead of collapsing between voltage bursts) and the V state will eventually replace the Hs state over the whole area of the device. At lower driving voltages, such as with bursts of 4 Vrms, the time for significant growth of the V state tends to be longer (e.g., is more than 100 ms at 4 Vrms). Here it is growth of the Ha states which tends to take over the Hs state – this is indicated by the purple areas in Fig. 2(b) – this condition is not suitable for phase modulator design, and therefore implies problematic effects in terms of Ha state formation limiting the duration of the stable Hs state.

To summarize, from the regions indicated in Fig. 2(b), we can choose appropriate voltage bursts and durations to optimise the lifetime of the Hs state. Furthermore, the repeating period of the burst voltage can also affect the lifetime of the Hs state, and we illustrate the longest burst duration for a suitable Hs state under a range of repeating periods (of 0.5 s, 1 s and 2 s) in Fig. 2(c). For all three periods the lifetime of the Hs state decreases as the burst driving voltage increases. As the repeat

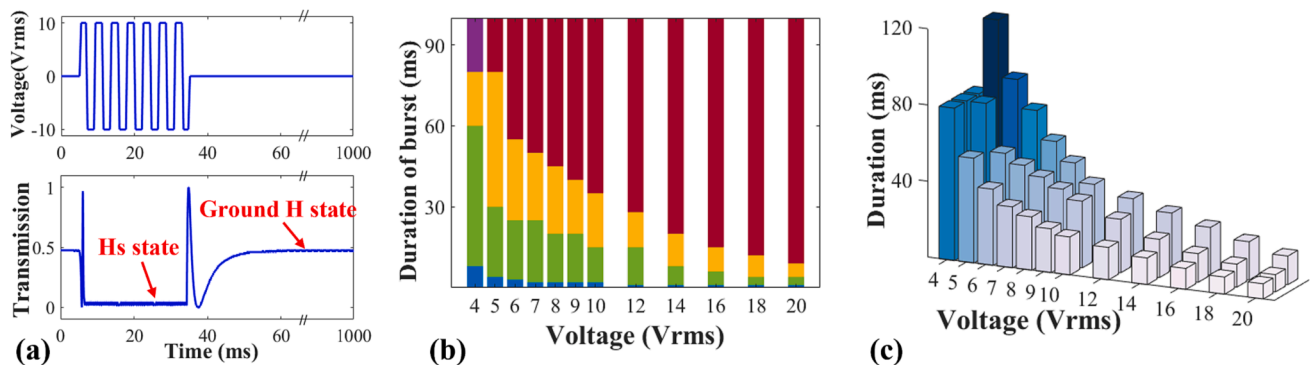


Fig. 2. Stability of the Hs state. (a) An illustration of the burst driving voltage and corresponding normalized transmission curve (note: the driving frequency during the burst was 1 kHz). (b) The various states that occur for different driving voltages and duration of the burst (blue – time to equilibrium state, green – Hs state, yellow mixture of V and Hs states, purple – problematic formation of Ha states, red – growth of the V state). (c) Illustration of how the lifetime of the Hs state can be affected by different repeat periods (the front, middle and back rows represent the periods 0.5 s, 1 s and 2 s, respectively).

period increases, the time needed for the Hs state formation remains the same, while the potential lifetime of the stable Hs state tends to become slightly longer – this is because any residual Ha and/or V state trapped around the spacer beads was more likely to entirely collapse when the time between burst driving voltage was longer. Therefore, for optical phase modulation applications, it was necessary to choose an appropriate relaxation period to avoid deleterious growth of the Ha and/or V state within the desired Hs state. In this work, the period of the burst driving voltage and relaxation time were set to 1 s and the duration of the bursts were chosen based on the stable Hs regime shown in Fig. 2(b).

C. Modelling the Optical Phase Modulation

To estimate the potential response time and phase modulation of the Hs state, we have modelled the LC director reorientation for different applied voltages and have predicted the resulting optical phase modulation based upon the director profiles – the results from these simulations have been used in subsequent sections to make comparisons with experimental results. To determine the LC director reorientation during transient switching of the Hs state in a pi-cell, a computer numerical model was implemented to solve the Ericksen–Leslie continuum equations [33]. There are two key parts to this: (i) the free energy density of the LC layer (which depends on the director configuration, LC elasticity, applied electric field and dielectric permittivities); (ii) the rate of energy dissipation during director reorientation (which depends on the LC viscosities, director reorientation rate and flow within the LC layer). Here we assume that the LC director remains within one plane and that its orientation is represented by an angle θ (the director tilt angle) which is a function of time and position across the LC layer (defined as the z -coordinate in what follows). The free-energy density (due to elastic and dielectric interactions) can then be written in terms of the director \mathbf{n} as

$$f = \frac{1}{2}K_{11}[\nabla \cdot \mathbf{n}]^2 + \frac{1}{2}K_{33}[\mathbf{n} \times (\nabla \times \mathbf{n})]^2 - \frac{1}{2}\Delta\epsilon\epsilon_0(\mathbf{n} \cdot \mathbf{E})^2 \quad (1)$$

where K_{11} , K_{22} and K_{33} are the splay, twist and bend elastic constants, $\Delta\epsilon$ is the dielectric anisotropy, and \mathbf{E} is the applied electric field. With the electric field along the z -direction this becomes

$$f = \frac{1}{2}K_{11}\cos^2\theta\left(\frac{\partial\theta}{\partial z}\right)^2 + \frac{1}{2}K_{33}\sin^2\theta\left(\frac{\partial\theta}{\partial z}\right)^2 - \frac{1}{2}\Delta\epsilon\epsilon_0\sin^2\theta E_z^2 \quad (2)$$

where E_z is the local electric field which is determined from the requirement for continuity in the z -component of the electric flux density.

To determine the director behaviour, we then need to solve

$$\frac{\partial}{\partial z}\left(\frac{\partial f}{\partial \theta'}\right) - \frac{\partial f}{\partial \theta} = \frac{\partial \mathcal{D}}{\partial \theta} \quad (3)$$

where \mathcal{D} is the dissipation function and the term on the righthand side of Eq. (3) can be written as

$$\frac{\partial \mathcal{D}}{\partial \theta} = (\alpha_3 - \alpha_2)\dot{\theta} + v_x'(\alpha_3\cos^2\theta - \alpha_2\sin^2\theta) \quad (4)$$

where α_2 and α_3 are the Leslie coefficients and v_x is a non-zero flow term. To solve Eq. (4) also requires knowledge of the flow, which is obtained from the Navier-Stokes equation. This leads to

$$\tilde{\sigma}_{xx} = \frac{\partial \mathcal{D}}{\partial v_x} = \frac{v_x'}{2} \left[2\alpha_1\sin^2\theta\cos^2\theta + \alpha_2(\cos^2\theta - \sin^2\theta) + 2\alpha_3\cos^2\theta + \alpha_4 + \alpha_5 \right] + \dot{\theta}(\alpha_3\cos^2\theta - \alpha_2\sin^2\theta) \quad (5)$$

where $\tilde{\sigma}_{xx}$ is the dynamic portion of the stress tensor, which can be obtained from the non-slip boundary conditions and the knowledge that it is independent of the z -coordinate, α_1 , α_2 , α_3 , α_4 and α_5 are Leslie coefficients.

This system of equations is solved using a simple finite difference approach, with a regular grid in the z -direction. As noted above, non-slip boundary conditions are used for the flow component. Additionally, the LC director tilt is fixed at the surfaces (here a small symmetric pre-tilt is used). This then allows the simulation of $\theta(z, t)$. To determine the resulting optical phase modulation the component of the LC refractive index parallel to the rubbing direction is calculated from the director profile

$$n_{\text{effective}}(z, t) = \frac{n_e n_o}{\sqrt{n_e^2 \sin^2\theta + n_o^2 \cos^2\theta}} \quad (6)$$

where n_o and n_e are the ordinary and extraordinary refractive indices, respectively. Eq. (6) can then be (numerically) integrated across the device thickness to determine a net retardation and hence an optical phase shift

$$\phi = \frac{2\pi}{\lambda} \int_0^d n_{\text{effective}}(z, t) \cdot dz - \phi_0 \quad (7)$$

where ϕ_0 is a chosen reference phase. The parameter values we used in this study were taken from the literature [33]. Specifically, these parameters were $K_{11} = 11.1$ pN, $K_{33} = 17.1$ pN, $\epsilon_{\perp} = 5.4$, $\epsilon_{\parallel} = 17.4$, $n_o = 1.5$, $n_e = 1.72$ and the wavelength was set to $\lambda = 632.8$ nm. The Leslie coefficients used in the model were $\alpha_1 = -21$ mPa·s, $\alpha_2 = -282$ mPa·s, $\alpha_3 = -1$ mPa·s, $\alpha_4 = 225$ mPa·s and $\alpha_5 = 92$ mPa·s, taken from [33].

To estimate the potential optical phase modulation, we consider an LC layer with small symmetric surface pre-tilt which is driven into a transient Hs state by the sudden application of a large electric field – the resulting director profile is then near homeotropic through the bulk of the LC layer, with thin transition regions near each surface and a thin transition region in the centre of the layer. In the limit of very large electric fields, the transition regions become vanishingly thin. When the applied field is removed the director profile begins to relax back towards the ground H state – initially this happens by the growth of boundary layers from each surface, and the growth of boundary layers from the central transition region. This initial behaviour is largely independent of the device thickness. The resulting director profile leads to a modulation in the optical phase of transmitted light. It is this stage which is critical in understanding the limits in available phase modulation speed because the “switch on” stage can be made fast by being driven with a sufficient electric field amplitude, but the “switch off” stage is limiting due to the balance between elasticity, viscosity and flow in the director reorientation. For the above parameters the resulting optical phase modulation was found to occur in 1 ms and is illustrated in the [Supplementary Information \(Supplementary Information S1\)](#) – this indicates the potential for greater than π phase modulation in transmission, which corresponds to greater than 2π phase modulation potential in a standard SLM reflective geometry, within a 1 ms time scale.

3. Experimental method

To experimentally investigate the fast switching and phase modulation of the Hs state in a nematic pi-cell, a phase-shifting Michelson interferometer was assembled as shown in Fig. 3. Light from a helium–neon laser with wavelength of 632.8 nm (Thorlabs, HNL050L) passed through a neutral density filter to a non-polarizing beam splitter, which divided the light into two paths: the signal path and the reference path. The pi-cell device was placed in the signal path and the LC device was driven by a function generator (Multicomp PRO, MP750510). By applying a periodical burst voltage driving waveform, as shown in Fig. 4 (a), there was a continuous optical phase response, where the device was driven into the Hs state and the phase was modulated with 1 ms pulses, which was then repeated every 1 s. The reference path contained a half-waveplate between two quarter-wave plates, which was rotated smoothly using a motor (PRM1Z8/M) to rotate the half-wave plate by 90°

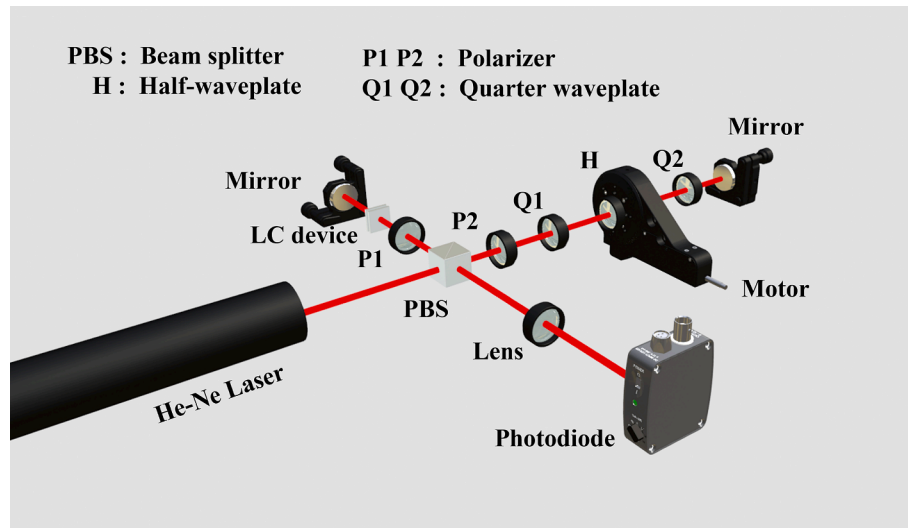


Fig. 3. Measuring the optical phase modulation of a nematic pi-cell in the Hs state. A phase-shifting Michelson interferometer was used to measure the phase modulation. One path of the interferometer contained the LC device to produce the phase delay to be measured, while the other path included two quarter-wave plates and a rotating half-wave plate to produce a continuous phase shift.

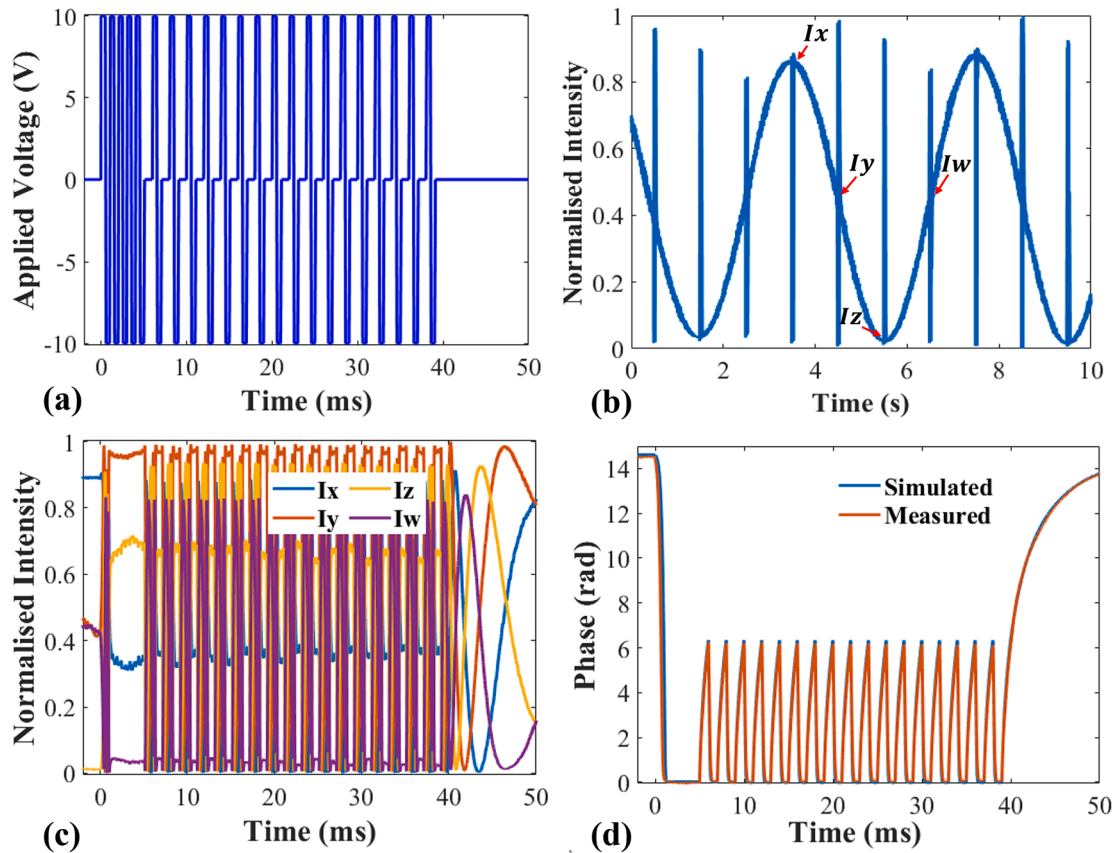


Fig. 4. Extracting the phase modulation of a nematic pi-cell in the Hs state. (a) The burst driving voltage applied to the nematic pi-cell, which consisted of a 40 ms operating period repeated every 1 s. (b) The interference results from the reference wave and signal wave, which contains the phase modulation of the LC device. (c) Enlarged view of the signal at the four key positions of the phase ramp. (d) Extracted experimental phase modulation of the nematic LC pi-cell in the Hs state using Eq. (10) demonstrating that the phase results are stable and show good consistency with the simulated results.

in 4 s, producing a continuous phase shift in the reference wave with a 2π phase shift period of 4 s [34]. Further details are given in the [Supplementary Information \(Supplementary Information S2\)](#). The light from the two paths of the interferometer were then re-combined by the beam splitter to generate an interference signal that was recorded by a photodiode (Thorlabs, PDA36A-EC, Si Amplified Detector 350–1100 nm).

The resulting interference signal is therefore the result of the overlapped interference of the optical phase shift from the switched Hs state of the LC device repeated in 1 s with the phase shift of the reference wave with a period of 4 s. Within each “period” of the reference wave there are four places where the phase shift from the burst driven Hs state can be observed. With an analogue-to-digital (A2D) converter, the

received light intensity can be acquired, shown in Fig. 4(b). The interference light signal received by the photodiode can be expressed as:

$$E = A(t)\cos(\omega t + kt) + B(t)\cos(\omega t + \varphi(t) + \Delta), \quad (8)$$

and the resulting intensity can be expressed as:

$$I = \frac{(A(t))^2}{2} + \frac{(B(t))^2}{2} + A(t)B(t)\cos(kt + \varphi(t) + \Delta) \quad (9)$$

where ω is the angular frequency of the light, k is the effective wave number of the phase shift in the reference light wave, kt represents the continuous phase shift produced by the rotating half-wave plate, $\varphi(t)$ is the phase modulation induced by the LC device, Δ is the optical path difference between the two arms and is not well defined and can also change over time (e.g., due to minor air movement etc.), $A(t)$ is the amplitude of the reference beam path and is near constant, $B(t)$ is the amplitude of signal light beam and it has residual amplitude modulation caused by the LC device.

Considering four step phase shifted intensity measurements, the required phase shifts, $kt + \Delta$, are equal to $n\pi$, $\frac{\pi}{2} + n\pi$, $\pi + n\pi$, and $\frac{3\pi}{2} + n\pi$. Based on the 4-step phase-shifting algorithm [35,36], the optical phase modulation, $\varphi(t)$, can then be extracted through:

$$\varphi(t) = \arctan\left[\frac{I_w(t) - I_y(t)}{I_x(t) - I_z(t)}\right] \quad (10)$$

where I_x , I_y , I_z , and I_w represent the intensity at four chosen points.

It also needs to be clarified that any intensity fluctuations introduced by small errors in the retardation of the half-wave plate are minimal (by careful selection of the waveplate used), and the measured amplitude modulation of the LC device is below 4% here. Therefore, neither of these cause a calculation error in the phase modulation.

Prior to extracting the phase, an initial experiment was performed to measure the transmission behaviour during the burst voltage. The transmission-time behaviour can quickly provide us with an estimate of the phase modulation expectation. Additionally, a transmission-voltage curve can be measured to confirm the device thickness. In this case, the pi-cell was placed between crossed polarizers with the rubbing direction at 45° to the polarizer axis. The light from the laser passed through a polarizer, LC device and another orthogonal polarizer in turn, before it was finally received by the photodiode. By applying the burst driving voltage to the device (as illustrated in Fig. 4(a)), a transmission-time curve can be obtained. The received intensity I can then be written as:

$$I = \frac{1}{2} \bullet \sin^2(2\chi) \bullet \sin^2\left(\frac{\Delta\varphi}{2}\right), \quad (11)$$

where χ is 45° in this setup representing the rotation angle of the device relative to the polarizer axis, $\Delta\varphi$ is the phase difference $\Delta\varphi = \frac{2\pi\Delta n_{eff}d}{\lambda}$, Δn_{eff} is the effective birefringence of the modulated LC device, d is the cell gap and λ is the wavelength of the polarized light incident on the cell. Similarly, by applying a gradually increasing square wave (1 kHz frequency is used here) and recording the transmission, the transmission-voltage curve can be observed. The results from these are included in the [Supplementary Information \(Supplementary Information S3\)](#) and indicate that: (1) the LC layer thickness was $3.73 \mu\text{m}$ (with a small pre-tilt of around 4°); and (2) by modulating the signal as illustrated in Fig. 4(a) a useful level of phase modulation is expected in the Hs state.

We now aim to measure the optical phase modulation in the LC device in the Hs state using the phase-shifting Michelson interferometer method outlined above. The applied burst driving voltage with operating period of 40 ms was repeated in every 1 s, shown in Fig. 4(a). This signal consisted of a “priming stage” of a $\pm 10 \text{ V}$ 1 kHz square wave for 5 ms (which drives the devices into the Hs state) followed by a “modulation stage”, where this drive voltage was repeatedly turned on for 1 ms and then off for 1 ms for the next 35 ms, followed by a “relaxation stage”

where no voltage was applied for the rest of the 1 s, to allow the LC device to return to the ground H state. The rotating half-wave plate provided a phase shift in the reference wave with a 2π periodicity of 4 s. With appropriate synchronization, the interference signal received by the photodiode was of the type shown in Fig. 4(b), where the vertical burst signal in the sine wave are the effects of the phase responses induced by the LC device repeated every 1 s. Following the approach outlined above, the signals around the four key points were chosen and extracted, as shown in Fig. 4(c). Using the 4-step phase-shifting algorithm represented by Eq. (10), the phase modulation was then extracted and is shown in Fig. 4(d), where the horizontal axis is the time scale, and the vertical axis is the phase modulation from the LC device. It is evident that a stable 2π phase modulation was achieved in 1 ms in the Hs state, and the measured phase modulation correlates well with our results from simulations for an LC layer thickness of $3.73 \mu\text{m}$ (the other device parameters were as listed above).

4. Experimental results

To further explore the phase modulation capability of the nematic pi-cell in the Hs state, the following experiments were conducted. Firstly, since the available phase modulation is related to the amplitude of the applied voltage, it was necessary to investigate the relationship between the driving voltage and the optical phase response of the device in the Hs state. To do this, a driving signal of the same form as that illustrated in Fig. 4(a) was used, with a priming stage of a 1 kHz square wave, followed by a modulation stage where the driving signal was repeatedly on for 1 ms and then off for 1 ms, followed by a relaxation stage with no voltage signal applied. By adjusting the amplitude of the 1 kHz voltage from 6 Vrms to 20 Vrms, the corresponding phase modulation was measured, as shown in Fig. 5(a). In each case the resulting optical phase modulation signal is offset to zero for the equilibrium Hs state present after the priming stage. It is seen that as the driving amplitude increases, the phase modulation depth also increases and the switching on speed also becomes faster. The increased available phase modulation at higher voltage is because when a larger voltage is applied the internal electric field then leads to a larger region of the LC director being parallel to the electric field and thus the transition regions (boundary layers) at the surfaces and in the centre of the device in the Hs state are thinner – when the field is removed this then produces a larger phase modulation within 1 ms.

The resulting available phase modulation as a function of voltage within a period of 1 ms is plotted in Fig. 5(b), together with the simulated response. It can be seen that the available phase modulation increases as the voltage increases, apparently tending towards an asymptote at higher voltages. Importantly, 2π optical phase modulation within 1 ms is available with a driving voltage of 10 Vrms, and when the voltage is above 10 Vrms the corresponding phase modulation is larger than 2π in 1 ms. However, it is also important to note that when the applied voltage is higher, the lifetime of the Hs state is reduced due to the rapid growth of the V state, limiting the potential to exploit the optical phase modulation response (for example, here when the voltage is 20 Vrms, the useful Hs state lifetime becomes less than 10 ms). It is also interesting to observe that for higher drive voltages a plot of the available phase modulation in 1 ms as a function of the inverse of the voltage leads to a straight line behaviour, as seen in Fig. 5(c). This is likely to be due to the fact that the LC electric coherence length is inversely related to the electric field strength, which then dictates how thin the boundary layers at the surfaces are and how thin the transition region in the centre of the Hs layer is, with a corresponding influence on the available optical phase modulation.

In addition, by choosing a suitable hold voltage, the optical phase after 1 ms can be maintained – this illustrates nicely the great potential for addressing multiple optical phase levels using switching in the Hs state. In this case, after the priming period required to establish the Hs state, the switching waveform in the operating period consists of

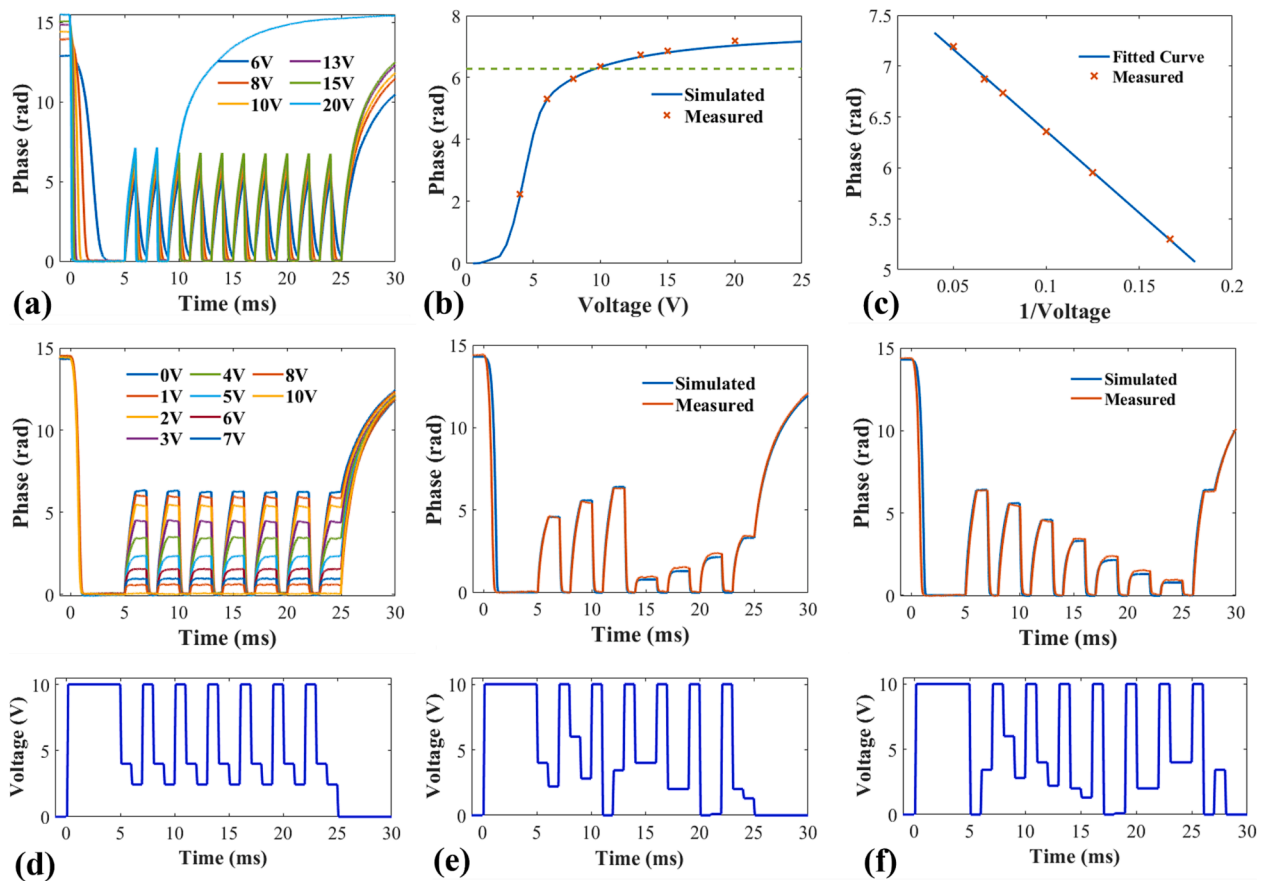


Fig. 5. Measured results: (a) phase modulation response as a function of time for various applied voltages with a 25 ms operation time (under 10 ms for 20 Vrms). (b) the relationship between the applied voltage and corresponding 1 ms phase modulation. (c) the 1 ms phase modulation at higher voltage is linearly dependent on the inverse of the applied voltage. (d) the phase modulation for different relax and hold voltages. The applied voltage waveform is presented in the lower plot. (e) and (f) continuous phase modulation (upper plot), and the corresponding applied voltage waveforms (lower plot).

driving, relaxing and holding in turn, where the driving voltage is fixed at 10 Vrms, the relaxation voltage is chosen to allow the establishment of a particular phase level in 1 ms, and the holding voltage is chosen to hold that phase level for a further 1 ms – therefore the corresponding hold voltage is varied as the relax voltage varies from 0 Vrms to 10 Vrms. The measured phase modulation curves are shown in Fig. 5(d), together with a plot of the rms voltage applied – this demonstrates that the optical phase can be set at any arbitrary chosen point in the range of 0 to 2π . The relationship between the hold voltage and the relax voltage and the optical phase state as a function of the relax voltage are shown in the [Supplementary Information \(Supplementary S4\)](#). To further demonstrate the optical phase modulation capability of the Hs state, the relax-hold voltage combination was varied in each operating period, the resulting phase modulation was found to be stable and shows good control, as shown in Fig. 5(e) and Fig. 5(f). Importantly, all of the measured results fit very well with the simulated ones. Therefore, it is well demonstrated that controllable optical phase modulation over a range of 0 to 2π can be achieved on millisecond time scales with a nematic LC pi-cell in Hs state.

5. Conclusions

In this paper, we use a burst driving voltage to obtain the Hs state in a nematic LC pi-cell device and investigate the effects of the amplitude and operating time on the stability for use as an optical phase modulator. The switching transition to the Hs state, and the required conditions for its stability are illustrated. Modelling based on Ericksen-Leslie theory indicated that useful optical phase modulation could be obtained in the

Hs state on a 1 ms timescale. To verify the model, a nematic LC (E7) was capillary filled into a pi-cell device. A phase measurement system based on a phase-shifting Michelson interferometer was established, which enabled the time-dependent optical phase variation to be obtained. The experimental results revealed that the Hs state can achieve a 2π optical phase modulation in 1 ms under a burst voltage of 10 Vrms at room temperature in a reflective device configuration (as commonly implemented in SLM technology). Further, multiple optical phase levels were achieved under various applied hold-relax voltage combinations. As the stability of the Hs state is limited, it cannot provide a truly continuous phase modulation with time, and thus further work is required to stabilize and preserve the Hs state, which would then provide a route to significantly enhance the capability of nematic based optical phase modulators.

CRediT authorship contribution statement

Linpei Xue: Methodology, Investigation, Formal analysis, Writing – original draft, Writing – review & editing. **Yihan Jin:** Conceptualization, Validation, Writing – review & editing. **Steve J. Elston:** Conceptualization, Investigation, Formal analysis, Validation, Supervision, Writing – review & editing. **Stephen M. Morris:** Conceptualization, Investigation, Supervision, Funding acquisition, Writing – review & editing.

Declaration of Competing Interest

The authors declare that they have no known competing financial

interests or personal relationships that could have appeared to influence the work reported in this paper.

Data availability

Data will be made available on request.

Appendix A. Supplementary data

Supplementary data to this article can be found online at <https://doi.org/10.1016/j.optlastec.2023.109773>.

References

- [1] K.M. Johnson, D.J. McKnight, I. Underwood, Smart spatial light modulators using liquid crystals on silicon, *IEEE Journal of Quantum Electronics* 29 (1993) 699–714.
- [2] S.T. Wu, A.M. Lackner, Mylar-film-compensated π and parallel-aligned liquid crystal cells for direct-view and projection displays, *Applied Physics Letters* 64 (1994) 2047–2049.
- [3] Y.-H. Lee, D. Franklin, F. Gou, G. Liu, F. Peng, D. Chanda, S.-T. Wu, Two-photon polymerization enabled multi-layer liquid crystal phase modulator, *Scientific Reports* 7 (2017) 16260.
- [4] S.T. Wu, C.S. Wu, High-speed liquid-crystal modulators using transient nematic effect, *Journal of Applied Physics* 65 (1989) 527–532.
- [5] Z. He, F. Gou, R. Chen, K. Yin, T. Zhan, S.-T. Wu, Liquid crystal beam steering devices: Principles, recent advances, and future developments, *Crystals* 9 (2019) 292.
- [6] C. Maurer, A. Jesacher, S. Bernet, M. Ritsch-Marte, What spatial light modulators can do for optical microscopy, *Laser & Photonics Reviews* 5 (2011) 81–101.
- [7] Y. Deng, C.-H. Huang, B. Vinoth, D. Chu, X.-J. Lai, C.-J. Cheng, A compact synthetic aperture digital holographic microscope with mechanical movement-free beam scanning and optimized active aberration compensation for isotropic resolution enhancement, *Optics and Lasers in Engineering* 134 (2020) 106251.
- [8] S.J. Woltman, G.D. Jay, G.P. Crawford, Liquid-crystal materials find a new order in biomedical applications, *Nature Materials* 6 (2007) 929–938.
- [9] A. Jesacher, C. Maurer, A. Schwaighofer, S. Bernet, M. Ritsch-Marte, Near-perfect hologram reconstruction with a spatial light modulator, *Optics Express* 16 (2008) 2597–2603.
- [10] Z. Zhang, Z. You, D. Chu, Fundamentals of phase-only liquid crystal on silicon (LCOS) devices 3 (2014) e213–e.
- [11] N.A. Clark, S.T. Lagerwall, Submicrosecond bistable electro-optic switching in liquid crystals, *Applied Physics Letters* 36 (1980) 899–901.
- [12] A.K. Srivastava, V.G. Chigrinov, H.S. Kwok, Ferroelectric liquid crystals: Excellent tool for modern displays and photonics, *Journal of the Society for Information Display* 23 (2015) 253–272.
- [13] J. Fünfschilling, M. Schadt, Fast responding and highly multiplexible distorted helix ferroelectric liquid-crystal displays, *Journal of Applied Physics* 66 (1989) 3877–3882.
- [14] V. Pertuis, J. Patel, Twisted smectic structure for gray scale modulator, *Ferroelectrics* 149 (1993) 193–205.
- [15] J. Patel, R.B. Meyer, Flexoelectric electro-optics of a cholesteric liquid crystal, *Physical Review Letters* 58 (1987) 1538.
- [16] J.A. Fells, X. Wang, S.J. Elston, C. Welch, G.H. Mehl, M.J. Booth, S.M. Morris, Flexoelectro-optic liquid crystal analog phase-only modulator with a 2π range and 1 kHz switching, *Optics Letters* 43 (2018) 4362–4365.
- [17] P.S. Salter, S.J. Elston, P. Raynes, L.A. Parry-Jones, Alignment of the uniform lying helix structure in cholesteric liquid crystals, *Japanese Journal of Applied Physics* 48 (2009) 101302.
- [18] C.-H. Yu, P.-C. Wu, W. Lee, Polymer stabilization of uniform lying helix texture in a bimesogen-doped cholesteric liquid crystal for frequency-modulated electro-optic responses, *Materials* 15 (2022) 771.
- [19] X. Wang, J.A. Fells, T. Ali, J.-D. Lin, C. Welch, G.H. Mehl, T.D. Wilkinson, M. J. Booth, S.M. Morris, S.J. Elston, Transmissive flexoelectro-optic liquid crystal optical phase modulator with 2π modulation, *AIP Advances* 10 (2020) 055011.
- [20] P.J. Bos, K.R. Koehler/ Beran, The pi-cell: a fast liquid-crystal optical-switching device, *Molecular Crystals and Liquid Crystals* 113 (1984) 329–339.
- [21] C.C. Tartan, S.J. Elston, Asymmetric director structures and flexoelectricity in nematic pi-cell devices, *Applied Physics Letters* 107 (2015) 081902.
- [22] S.H. Lee, T.J. Kim, G.-D. Lee, T.-H. Yoon, J.C. Kim, Geometric structure for the uniform splay-to-bend transition in a π -cell, *Japanese Journal of Applied Physics* 42 (2003) L1148.
- [23] Y. Jin, S.J. Elston, J.A. Fells, M.J. Booth, C. Welch, G.H. Mehl, S.M. Morris, Millisecond optical phase modulation using multipass configurations with liquid-crystal devices, *Physical Review Applied* 14 (2020) 024007.
- [24] H. Kikuchi, H. Yamamoto, H. Sato, M. Kawakita, K. Takizawa, H. Fujikake, Bend-mode liquid crystal cells stabilized by aligned polymer walls, *Japanese journal of applied physics* 44 (2005) 981.
- [25] P. Brimicombe, S. Elston, E. Raynes, Dynamic properties of polymer stabilised pi-cells, *Molecular Crystals and Liquid Crystals* 476 (2007), 165/[411]-179/[425].
- [26] F.-S.-Y. Yeung, H.-S. Kwok, Fast-response no-bias-bend liquid crystal displays using nanostructured surfaces, *Applied Physics Letters* 88 (2006) 063505.
- [27] F.S. Yeung, Y.W. Li, H.-S. Kwok, Pi-cell liquid crystal displays at arbitrary pretilt angles, *Applied Physics Letters* 88 (2006) 041108.
- [28] P. Brimicombe, E. Raynes, The influence of flow on symmetric and asymmetric splay state relaxations, *Liquid Crystals* 32 (2005) 1273–1283.
- [29] C.-H. Lee, E. Raynes, S. Elston, The effect of high voltage on the bend transition in Pi-cells, *Applied Physics Letters* 97 (2010) 153501.
- [30] P. Brimicombe, E. Raynes, Symmetric H state lifetime in splayed nematic liquid crystal devices, *Applied Physics Letters* 89 (2006) 031121.
- [31] B.-R. Yang, S.J. Elston, P. Raynes, H.-P.-D. Shieh, Investigation of the transient symmetric H state in a pi cell, *Applied Physics Letters* 91 (2007) 071119.
- [32] S.J. Elston, Flexoelectricity in nematic domain walls, *Physical Review E* 78 (2008) 011701.
- [33] P. Brimicombe, L. Parry-Jones, S. Elston, E. Raynes, Modeling of dual frequency liquid crystal materials and devices, *Journal of Applied Physics* 98 (2005) 104104.
- [34] R.N. Shagam, J.C. Wyant, Optical frequency shifter for heterodyne interferometers using multiple rotating polarization retarders, *Applied Optics* 17 (1978) 3034–3035.
- [35] K. Creath, V phase-measurement interferometry techniques, *Progress in Optics*, Elsevier (1988) 349–393.
- [36] G. Stoilov, T. Dragostinov, Phase-stepping interferometry: five-frame algorithm with an arbitrary step, *Optics and Lasers in Engineering* 28 (1997) 61–69.